Langmuir

Universitat d'Alacant
Universidad de Alicante

Subscriber access provided by Universidad de Alicante

Article

Assessment of CO2 adsorption capacity on activated carbons by a combination of batch and dynamic tests

Marco Balsamo, Ana Silvestre-Albero, Joaquin Silvestre-Albero, Alessandro Erto, Francisco Rodriguez-Reinoso, and Amedeo Lancia

Langmuir, **Just Accepted Manuscript** • DOI: 10.1021/la500780h • Publication Date (Web): 30 Apr 2014

Graphical Abstract

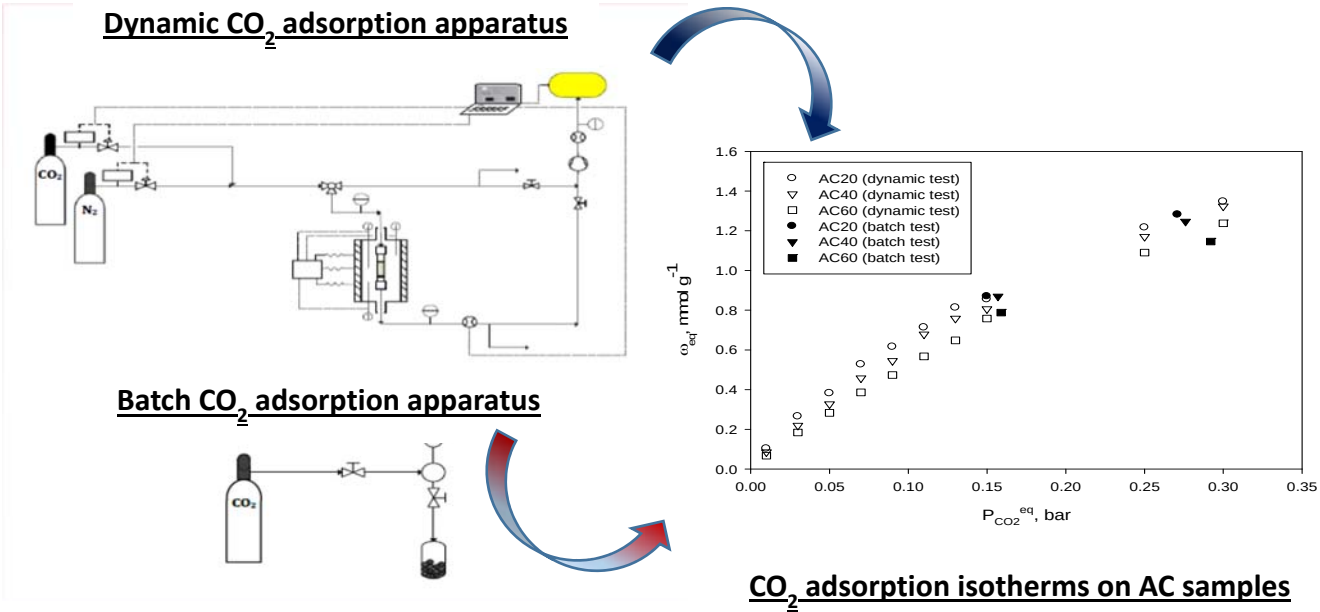

Assessment of CO_2 adsorption capacity on activated carbons by a combination of batch and dynamic tests

Marco Balsamo[1], *Ana Silvestre-Albero*[2], *Joaquín Silvestre-Albero*[2], *Alessandro Erto*[1*], *Francisco Rodríguez-Reinoso*[2], *Amedeo Lancia*[1]

[1] Dipartimento di Ingegneria Chimica, dei Materiali e della Produzione Industriale, Università degli Studi di Napoli Federico II, Piazzale Vincenzo Tecchio 80, 80125 Napoli, Italy

[2] Laboratorio de Materiales Avanzados, Departamento de Química Inorgánica, Instituto Universitario de Materiales, Universidad de Alicante, Ap. 99, E-03080 Alicante, Spain

Abstract

In this work, batch and dynamic adsorption tests are coupled for an accurate evaluation of CO_2 adsorption performance for three different activated carbons obtained from olives stones by chemical activation followed by physical activation with CO_2 at varying times, i.e. 20, 40 and 60 h. Kinetic and thermodynamic CO_2 adsorption tests from simulated flue-gas at different temperature and CO_2 pressure are carried out both in batch (a manometric equipment operating with pure CO_2) and dynamic (a lab-scale fixed-bed column operating with CO_2/N_2 mixture) conditions. The textural characterization of the activated carbon samples shows a direct dependence of both micropore and ultramicropore volume on the activation time, hence AC60

[*] Corresponding author. Tel.: +39 081 7682236; fax: +39 081 5936936.
E-mail address: aleserto@unina.it (A. Erto).

has the higher contribution. The adsorption tests conducted at 273 and 293 K showed that, when CO_2 pressure is lower than 0.3 bar, the lower the activation time the higher CO_2 adsorption capacity and a ranking $\omega_{eq}(AC20)>\omega_{eq}(AC40)>\omega_{eq}(AC60)$ can be exactly defined when T= 293 K. This result can be likely ascribed to a narrower pore size distribution of the AC20 sample, whose smaller pores are more effective for CO_2 capture at higher temperature and lower CO_2 pressure, the latter representing operating conditions of major interest for decarbonation of a flue-gas effluent. Moreover, the experimental results obtained from dynamic tests confirm the results derived from the batch tests in terms of CO_2 adsorption capacity. It is important to highlight that the adsorption of N_2 on the synthesized AC samples can be considered negligible. Finally, the importance of a proper analysis of characterization data and adsorption experimental results is highlighted for a correct assessment of CO_2 removal performances of activated carbons at different CO_2 pressure and operating temperature.

Keywords: CO_2; adsorption; activated carbon; carbon capture and storage; global warming

1. Introduction

CO_2 is unanimously considered as the primary greenhouse gas emitted through human activities, responsible for about 60% of increased greenhouse effect and climate change[1,2]. The combustion of fossil fuels for the generation of heat and power energy is the main CO_2 emission source. Although many efforts are currently devoted to develop new and cleaner technologies, such as chemical looping combustion, new gasification technologies for power plants and hydrogen-based fuel cells[2,3], an immediate and effective CO_2 mitigation can be pursued by the adoption of appropriate post combustion technologies. The use of porous solids for CO_2 capture

is gaining crescent interest within the Carbon Capture and Storage (CCS) strategy aimed at a short-term reduction of CO_2 industrial emissions. Currently, several techniques are applied for the separation and capture of CO_2, which include amine-based absorption, membrane separation, cryogenic distillation and adsorption process[4-6]. An appropriate CO_2 capture technology should be effective, low cost, environmentally benign and easily applicable. In this context, adsorption technology represents a promising solution, which can be easily implemented in existing power plants. Moreover, it is a well-established technique which can be adopted for the removal of different classes of pollutants from both gaseous and liquid streams, thanks to a high versatility and general low maintenance costs[7-12]. Although different classes of adsorbents are extensively investigated in the pertinent literature, the use of activated carbons (ACs) for CO_2 capture has a great appeal thanks to their tuneable porous structure, a wide adsorption spectrum and relatively limited costs[7,8,13,14]. In addition, CO_2 adsorption on ACs has been demonstrated to be a reversible process, hence CO_2 recovery and AC regeneration can be simultaneously pursued by a desorption process[15-18].

Activated carbons can be manufactured starting from various carbonaceous precursors[17,19-21]. In particular, lignocellulosic materials are characterized by general low-costs and abundant availability, which can allow a significant saving in adsorbent production and process management. Many efforts have been expended in the development of adsorbent materials from agricultural wastes[21-25] and, specifically, to define the optimal textural as well as chemical properties to maximize CO_2 capture[26-28]. At the current state-of-the-art, there is a general accordance in the literature to consider the increase in CO_2 adsorption capacity, under flue-gas simulated conditions (CO_2 partial pressure typically lower than 0.15 bar), as closely related to a high total or micropore volume coupled with a narrower micropore size distribution shifted

towards ultramicropores[13,26,29-31]. In particular, Sun and co-workers[29] elucidated the main functional dependencies by a dedicated statistical analysis applied to a large set of activated carbons, in which the correlation degree between CO_2 adsorption capacity and textural properties was determined. Similarly, Yin and co-workers[31] analysed a large number of experimental works present in the literature and concluded that the surface area of activated carbon is not the determining factor for CO_2 adsorption, while ultramicropores have a significant influence.

On the other side, Balsamo and co-workers[32] pointed out that micropore diffusion is the limiting step of adsorption process carried out in fixed-bed column. Simultaneously, they highlighted the positive effect exerted by mesopores in the enhancement of CO_2 adsorption rate, as already stated by different authors, which worked with volumetric (manometric) apparatuses operated in batch mode[11,29].

Despite the large number of studies focused on the determination of the correlations between activated carbon properties and CO_2 capture performances, few studies are performed in simulated flue-gas streams[15,17,29,32]. In addition, the current literature is still lacking of thorough studies on CO_2 adsorption onto activated carbons in dynamic conditions, as most of the experimental works are carried out in volumetric/gravimetric apparatuses. Even less studies are available in which the adsorption of CO_2 is investigated simultaneously from simulated flue-gas, in dynamic systems, and as a function of the main operational parameters (e.g. gas temperature, CO_2 concentration, etc.)[33-35].

The goal of this work is an experimental analysis of CO_2 adsorption onto activated carbons (AC), produced starting from olive stones, through a combined set of batch and dynamic tests. A microstructural characterization of the AC samples by N_2 and CO_2 adsorption was carried out aimed at assessing the contribution of mesopores, micropores and narrow micropores. Kinetic

and thermodynamic CO_2 adsorption tests at different CO_2 pressure and temperature were performed both in batch (glass-made manometric adsorption equipment operating with pure CO_2) and in dynamic (a lab-scale fixed-bed column operating with CO_2/N_2 mixture) conditions, for a thorough comparison. The complementarity of batch and dynamic experiments was highlighted in order to pursue a correct determination of CO_2 adsorption capacity and to assess the factors affecting the CO_2 capture in operating conditions typical of a flue-gas (in terms of temperature and CO_2 concentration).

2. Materials and methods

2.1. Activated carbon samples

Three AC samples were synthesized starting from the same lignocellulosic precursor (i.e. olive stones) according to the procedure reported by Silvestre-Albero and co-workers[36]. A combination of chemical and physical activation processes was adopted which involved the impregnation with an aqueous solution of $ZnCl_2$ at 358 K and a heat treatment under a N_2 flow at 773 K; this was followed by a physical activation performed with CO_2 (100 cm^3 min^{-1}) at 1098 K using different periods of time, i.e. 20, 40 and 60 h, which gave rise to the different labelled materials (i.e. AC20, AC40 and AC60, respectively).

A particle size range 1.00-2.36 mm was selected for all the experimental runs by mechanical sieving.

The textural properties of the synthesized AC samples were determined in a fully automated manometric equipment, the N_2Gsorb-6 porosimeter (www.g2mtech.com). Adsorption isotherms of N_2 and CO_2 were obtained at 77 K and 273 K, respectively. Before each experiment, the samples were outgassed at 423 K for 4 h under vacuum (10^{-8} bar) in order to remove humidity.

The main microstructural parameters of the AC samples were obtained from mathematical processing of N_2 and CO_2 adsorption isotherms according to the models commonly applied in the literature. In particular, the ‘‘apparent” surface area was obtained using the BET method. The micropore volume (V_o) was deduced from the N_2 adsorption data using the Dubinin–Raduskevitch (DR) equation, while the mesopore volume (V_{meso}) was obtained as the difference between the total pore volume (V_t) adsorbed at $P/P^0 \sim 0.95$ and the micropore volume (V_o). The pore volume corresponding to the narrow microporosity (V_n) was obtained after application of the DR equation to the CO_2 adsorption data at 273 K.

2.2 Kinetic batch adsorption experiments

Pure CO_2 batch adsorption kinetics on the AC samples was carried out at 293 K in a glass-made manometric adsorption equipment developed by the Laboratorio de Materiales Avanzados group. Experimental runs were performed at two different initial CO_2 pressures, namely 0.25 and 0.42 bar and employing 0.2 g of each AC tested. The adsorption kinetics was determined from the pressure decrease in the pressure transducer with time. Prior to the adsorption experiment, the sample was degassed under vacuum (10^{-7} bar) at 423 K for 4 h.

2.3. Dynamic adsorption experiments

The dynamic adsorption runs were carried out in a lab-scale fixed-bed column (length=0.13 m; inner diameter=0.02 m) made up of Pyrex glass. The fixed bed temperature was controlled by means of cylindrical shell Watlow band heaters, enveloped in a thermal insulating layer of ceramic fibres, and connected to EZ-PM® PID controllers (Watlow).

Two mass flow controllers (series El Flow Bronkhorst 201-CV) were used to generate a gas (N_2+CO_2) with 1-30% CO_2 concentration. Gas volumetric flow rate variations, occurring in the fixed bed as a consequence of CO_2 adsorption, were monitored by means of a mass flow meter series El Flow Bronkhorst 201-CV placed at the exit of the adsorption column.

A continuous NDIR (non-dispersive infrared) gas analyzer (AO2020 Uras 26 model provided by ABB) was adopted for the determination of CO_2 concentration. Finally, data acquisition and elaboration were performed by interfacing the analyser with a PC unit via LabView™ software.

Experimental tests in fixed-bed column were carried out by feeding the column, charged with a fixed adsorbent amount (i.e. 0.015 kg), with a 1.5 L min^{-1} gas stream (N_2+CO_2) at 293 K and 1 atm total gas pressure.

CO_2 dynamic adsorption results were processed to obtain the corresponding adsorption isotherms. As known, the material balance on CO_2 over the fixed-bed column leads to the determination of the equilibrium CO_2 adsorbed amount, ω_{eq} [mmol g^{-1}]:

$$\omega^{eq} = \frac{Q_{CO_2}^{in}\rho_{CO_2}}{mM_{CO_2}}\int_0^{t_{eq}}\left(1 - \frac{Q_{CO_2}^{out}(t)}{Q_{CO_2}^{in}}\right)dt \qquad (1)$$

where $Q_{CO_2}^{in}$ and $Q_{CO_2}^{out}$ are column inlet and outlet CO_2 volumetric flow rates, respectively; *m* is the mass of adsorbent; ρ_{CO2} [mg L^{-1}] represents CO_2 density (evaluated at 293 K and 1 bar); M_{CO2} is its molecular weight [mg $mmol^{-1}$].

A check on adsorption capacity was carried by desorption runs on spent AC samples. Pure N_2 was used as desorbing agent and the CO_2 outlet concentration was monitored by means of the NDIR analyzer. The desorption profiles were elaborated to obtain the total specific amount of CO_2 desorbed from the spent AC, ω_{des} [mmol g^{-1}], through a material balance, similar to Eq. (1):

$$\omega^{des} = \frac{\rho_{CO_2}}{mM_{CO_2}} \int_0^{t_{0.1}} Q_{CO_2}^{out}(t)dt \quad (2)$$

in which t0.1 is the time required to complete the desorption process, assumed as the one corresponding to the NDIR low detection limit (0.1% CO_2 by vol.). The maximum allowed discrepancy between ω_{eq} and ω_{des} was set at 5 %.

Further details about dynamic experimental apparatus and adsorption tests were reported in a previous work[17].

3. Results and discussion

3.1. Activated carbon textural characterization

The characterization of the textural properties of the AC samples included the realization of both N_2 and CO_2 adsorption isotherms at 77 K and 273 K respectively, in order to investigate all the dimensional ranges of AC porosity.

The N_2 adsorption isotherms, previously reported by Silvestre-Albero and co-workers[36], showed that all the AC samples are mainly microporous with a narrow knee at low relative pressure (Type I isotherms). Consequently, since it is generally accepted that CO_2 adsorption occurs by a micropore filling mechanism[28,37,38], pore size distribution (PSD) is expected to play a crucial role in determining CO_2 adsorption performances of the investigated AC samples.

In Figure 1, the PSD of all the AC samples, as derived from N_2 adsorption isotherms by application of the QSDFT (Quenched Solid Density Functional Theory), are depicted.

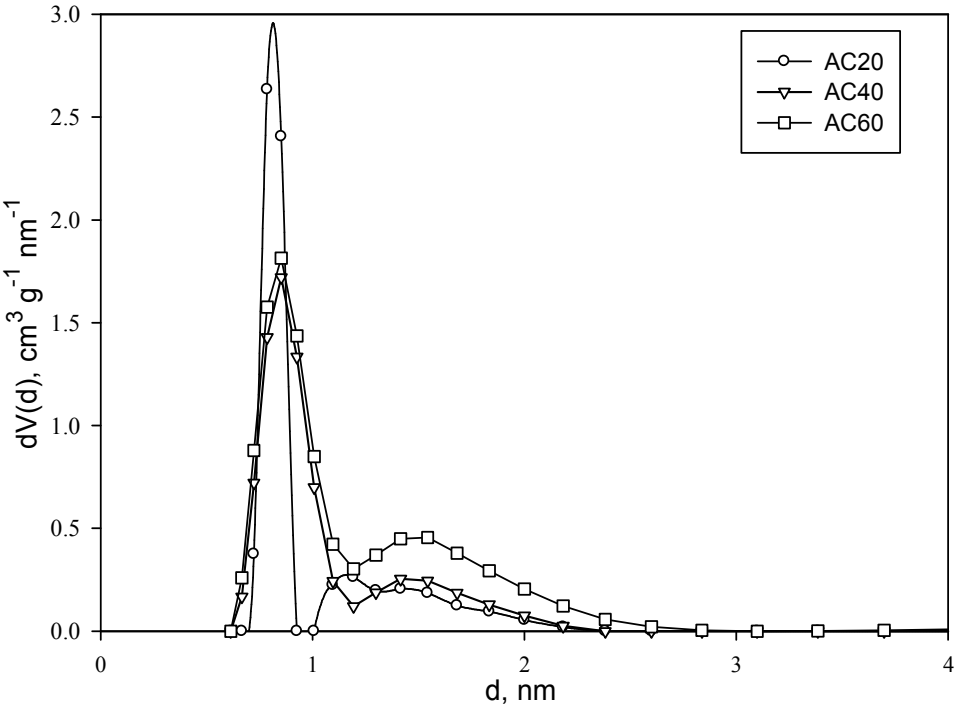

Figure 1. Pore size distribution of AC20, AC40 and AC60 samples obtained by QSDFT method (slit-shape equilibrium model) applied to N_2 adsorption isotherm at 77 K.

As it can be observed, the AC20 sample has the narrower PSD, mostly included in the range of narrow micropores (pore diameter < 10 Å). Differently, AC40 and AC60 samples have lower narrow micropore contribution, with a distribution shifted towards micropores of higher dimensions. In addition, AC60 sample shows a somewhat higher contribution of mesopores with respect to AC40 and, more, to AC20.

The analysis of the pertinent literature showed that microporous carbon materials with pores less than 1 nm are considered as the most suitable for CO_2 capture at ambient temperature and pressure[13,26,30,39]. Hence, in order to deepen the investigation of smaller pore sizes and their

effect on CO_2 adsorption, CO_2 adsorption isotherms at 273 K were realized for all the AC samples and reported in Figure 2.

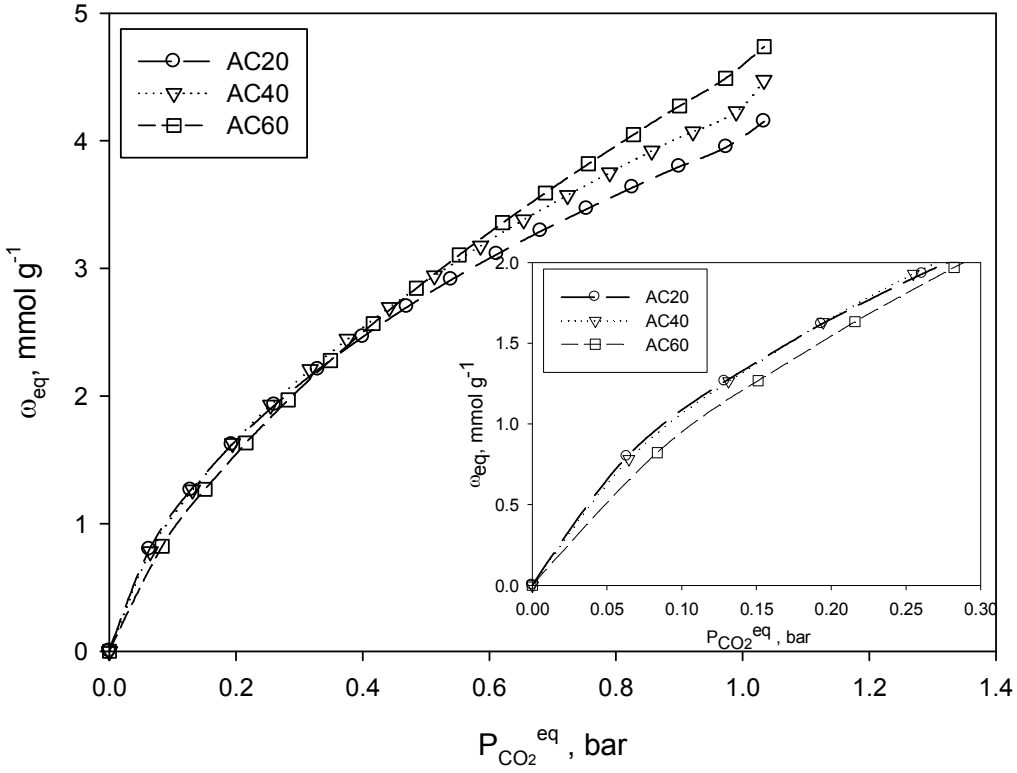

Figure 2. CO_2 adsorption isotherms at 273 K for AC20, AC40 and AC60 samples. The inset graph represent the magnification of the 0-0.3 bar region.

All the AC samples exhibit the expected isotherm shape and the adsorption capacity monotonically increases with CO_2 pressure and an asymptotic value is not reached in the investigated range.

All the parameters deriving from N_2 and CO_2 porosimetric analyses commonly adopted to fully characterize the textural properties of the AC samples are reported in Table 1.

	N_2 adsorption, 77 K				CO_2 adsorption, 273 K
Sample	S_{BET} (m^2/g)	V_o (cm^3/g)	V_{meso} (cm^3/g)	V_t (cm^3/g)	V_n (cm^3/g)
AC20	1253	0.46	0.07	0.53	0.36
AC40	1448	0.54	0.09	0.63	0.40
AC60	1983	0.70	0.23	0.93	0.45

Table 1. Textural parameters of AC20, AC40 and AC60 samples derived from N_2 and CO_2 adsorption isotherms at 77 K and 273 K, respectively

The application of the DR equation to N_2 and CO_2 isotherms allowed determining that a higher activation time resulted in both higher micropore (V_o) and narrow micropore (V_n) volumes, the increase of the former being more relevant. Coherently, also the BET surface area increased with the activation time, and the contribution of mesopores (V_{meso}) became significant only for AC60 sample, as already deducted by PSD analysis. A comparative analysis of the data reported in Table 1 shows that AC60 has the highest micropore volume (V_o), but AC20 has the highest fraction of narrower micropore (calculated as V_n/V_t ratio), as previously observed in Figure 1. Moreover, it can be stated that the activation treatment with CO_2 determines the opening of new micropores coupled with the broadening of the porosity, as testified by the increasing difference between micropores (V_o) and narrow micropores (V_n) as a consequence of a higher burn-off with activation time[13,36].

The results obtained so far would drive to the conclusion that AC60 is the most suitable sample for CO_2 adsorption. In fact, a higher micropore and narrow micropore contribution is commonly believed as a condition for the individuation of the sorbent with highest CO_2

adsorption capacity (ω_{eq}). As a matter of fact, this result is always verified as long as CO_2 pressure assumes values equal to 1 bar[13,19,26,30,31]. Coherently, data reported in Figure 2 confirms that for a CO_2 pressure of 1 bar a monotonic ranking $\omega_{eq}(AC60)>\omega_{eq}(AC40)>\omega_{eq}(AC20)$ exists. However, it is interesting to observe that for a CO_2 pressure < 0.3 bar, the ranking is almost inverted and becomes $\omega_{eq}(AC20)\approx\omega_{eq}(AC40)>\omega_{eq}(AC60)$. This result suggests a different energetic distribution of the active sites of the different AC samples, which favours the adsorption capacity of AC20 and AC60 for low and high CO_2 pressure, respectively. An overall analysis of the experimental results so far presented can be made following the Dubinin's micropore filling theory. The high adsorption potential determined in narrow micropores, which are mostly abundant in AC20 (cf. Figure 1) allows a more effective packing of CO_2 molecules even at low adsorbate partial pressures, thus explaining the higher CO_2 adsorption capacity of AC20 at low CO_2 pressures[13,32,39]. The AC40 and AC60 samples show an almost similar contribution of smaller micropores, even if the AC60 sample presents a sensibly higher contribution of wider micropores and mesopores (as confirmed by data reported in Table 1), these pores being favourably filled only at higher CO_2 partial pressures because of their lower adsorption potential[39,40]. On the basis of the reported PSD and from CO_2 adsorption data at 273 K (Figure 1), it can be deducted that the wider pores provide a higher contribution to CO_2 adsorption above a stated crucial value of CO_2 pressure.

These results assume an even greater importance when dealing with CO_2 capture from flue gas, in which CO_2 concentration is always largely lower than 30%. However, in this step, the analytical tests were performed in the fully automated manometric apparatus (cf. Section 2.1.) with pure CO_2 at different pressure and at 273 K. Hence, in order to go into the effect of

temperature and CO_2 partial pressure further investigations were carried out in different experimental conditions and reported in the following sections.

3.2. CO_2 adsorption kinetics in batch system

In order to extend the field of investigation of CO_2 adsorption onto the synthesized AC samples, new experimental runs were carried out at 293 K in a manometric apparatus. To this aim, kinetic batch tests were realized with pure CO_2 and for two different initial CO_2 pressure ($P^0_{CO_2}$) levels, namely 0.25 and 0.42 bar. The results are depicted in Figure 3A and 3B, respectively. It is worth to observe that the batch character of these tests leads to a variable CO_2 final equilibrium pressure which depends mainly on CO_2 equilibrium adsorption capacity, but also on slight variations in the initial pressure and in the mass of the adsorbent charged into the apparatus. Hence, for the sake of completeness, in Figure 3A-3B, the CO_2 equilibrium pressure ($P^{eq}_{CO_2}$) was reported for each experimental run.

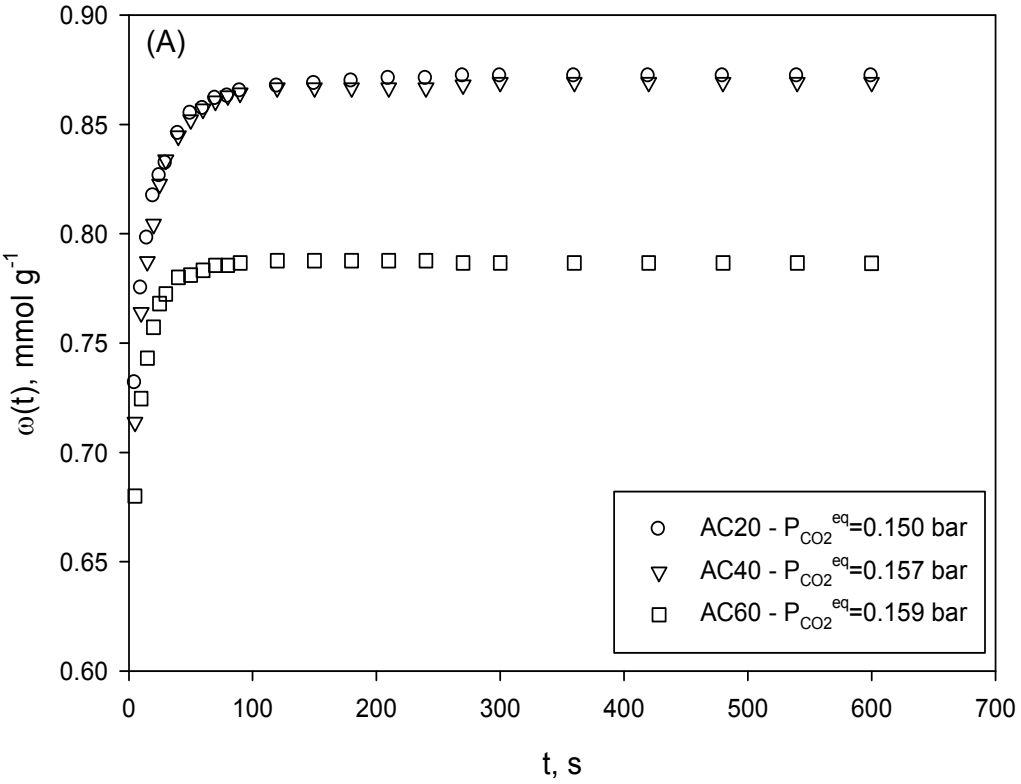
(A)
ω(t), mmol g-1
t, s
AC20 - P CO2 eq=0.150 bar
AC40 - P CO2 eq=0.157 bar
AC60 - P CO2 eq=0.159 bar

252

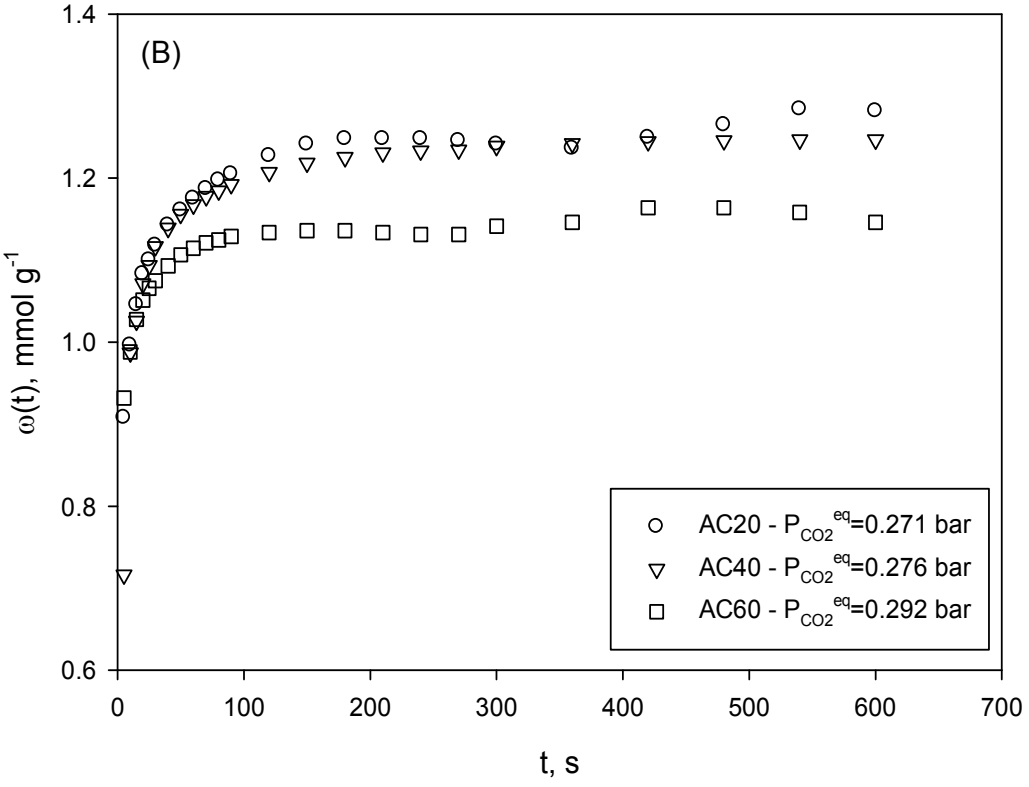
(B)
ω(t), mmol g-1
t, s
AC20 - P CO2 eq=0.271 bar
AC40 - P CO2 eq=0.276 bar
AC60 - P CO2 eq=0.292 bar

253

Figure 3. Pure CO_2 batch adsorption tests on AC samples at (A) $P^0_{CO_2}$ = 0.25 and (B) $P^0_{CO_2}$ = 0.42 bar. T= 293 K; adsorbent dose: 0.2±0.01 g

From Figure 3 it can be observed that, for both the CO_2 initial pressures investigated, CO_2 adsorption rate is higher for AC60, as testified by the lowest time taken to reach the final equilibrium adsorption capacity; on the other hand, differences between AC20 and AC40 are very slight. In Table 2, the equilibrium times (t_{eq}), as derived from experiments reported in Figure 3, are summarized:

	AC20	**AC40**	**AC60**
t_{eq} **(** $P^0_{CO_2}$ **=0.25 bar), s**	210	180	90
t_{eq} **(** $P^0_{CO_2}$ **=0.42 bar), s**	420	360	180

Table 2. Comparison between equilibrium time (t_{eq}) values obtained from batch adsorption tests for AC20, AC40 and AC60 at different CO_2 initial pressure ($P^0_{CO_2}$)

These results reflect the mesopore content of the AC samples, highest for AC60 and comparable for AC40 and AC20, which is commonly believed to exert a significant influence on CO_2 adsorption rate[13,32]. Moreover, the experimental results clearly demonstrate that in both the investigated experimental conditions AC60 has the lowest adsorption capacity while AC20 displays comparable (Figure 3A) or slightly better (Figure 3B) CO_2 removal performances at equilibrium, with respect to AC40. However, a rigorous analysis should take into account also

the differences in equilibrium pressure, which allows considering AC20 favoured with respect to AC40 also at lowest equilibrium pressure (Figure 3A). Hence, for the two tests conducted at CO_2 partial pressure <0.3 bar and T=293 K the new ranking of adsorption capacity is $\omega_{eq}(AC20)>\omega_{eq}(AC40)>\omega_{eq}(AC60)$. A comparison with the adsorption isotherm at T=273 K (Figure 2), equally realized with pure CO_2, confirms the exothermic character of CO_2 adsorption (as expected the amount adsorbed is lower at 293 K for all samples) but leads to a further important conclusion. An increase in temperature determines a reduction of the pore size diameter active towards CO_2 adsorption; in fact, at 293 K, the AC20 sample shows the highest difference in adsorption capacity with respect to AC40 and AC60 whereas these differences decrease at 273 K. This result is consistent with the experimental findings reported by Zhang and co-workers[41] which observed that at higher temperature stronger adsorption potentials, as those related with pore of smaller dimension, are required to avoid the adsorbate escaping from pores (due to their higher kinetic energy). It can be concluded that narrow micropores play a more relevant role at 293 K, with respect to 273 K, and low CO_2 pressures in determining higher pollutant capture performances for AC20 sorbent.

3.3. CO_2 adsorption in dynamic system

The above experimental results highlighted the substantial effect of temperature and CO_2 pressure on adsorption capacity of the investigated series of AC. In particular, the inversion of performance ranking observed for a pressure < 0.3 bar drives to further investigations in this range of pressures, which is consider of great interest because it includes those typical of a post-combustion CO_2 capture treatment. The new experimental runs were performed at T= 293 K in a

dynamic system represented by a fixed-bed column, in which a model flue-gas composed by CO_2+N_2 was fed.

The breakthrough profiles of CO_2 on AC20, AC40 and AC60 obtained at different CO_2 concentration in the feed (range 1-15% by vol.) are depicted in Figures 4 (A)-(H).

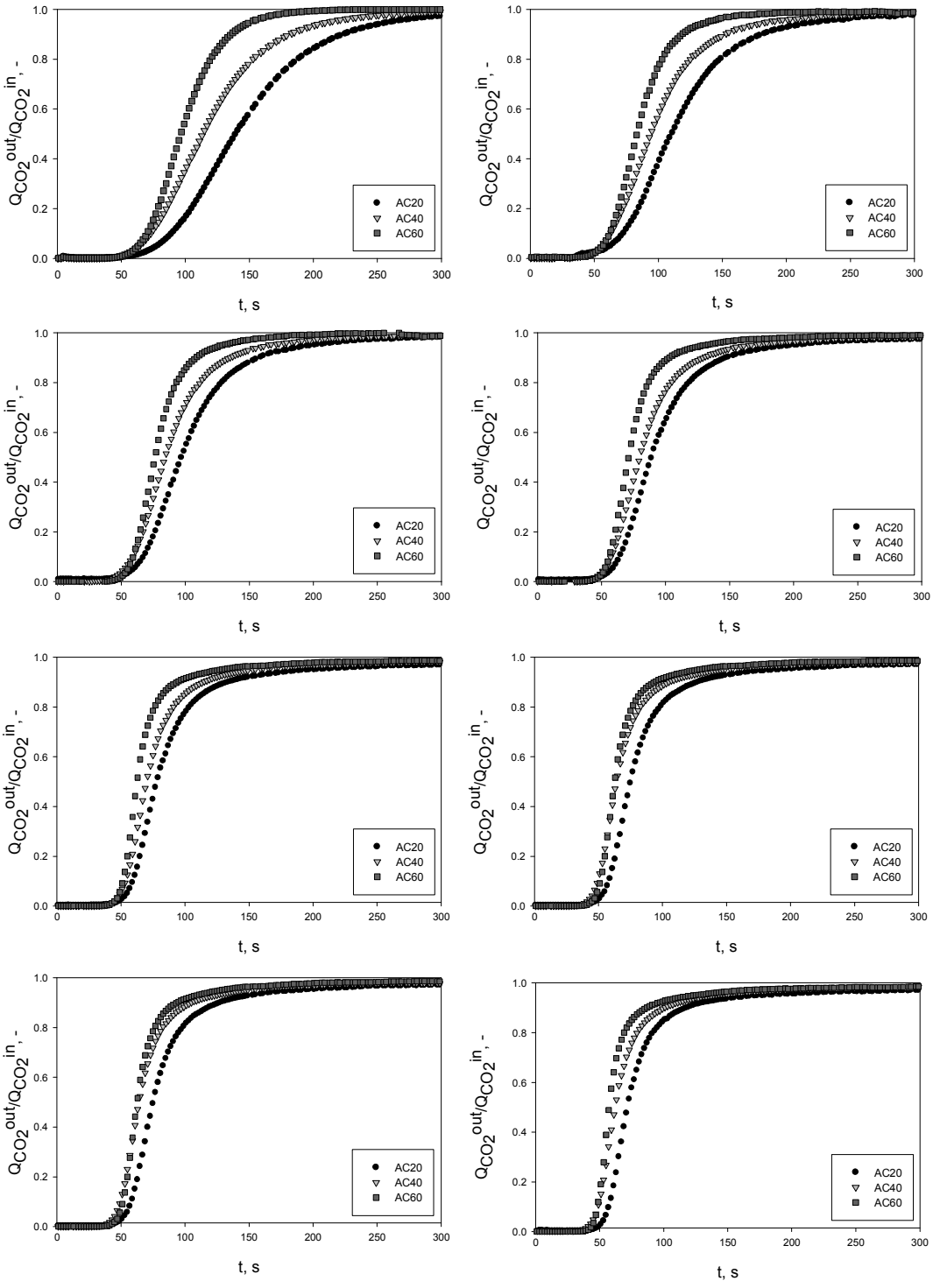

Figure 4. Breakthrough curves of CO_2 adsorption on AC20, AC40 and AC60 at different CO_2 concentration in the feed (balance N_2). A) 1%; B) 3%; C) 5%; D) 7%; E) 9 %; F) 11%; G) 13%; H) 15%. T= 293 K, P=1 bar.

The analysis of the dynamic adsorption patterns reveals that for all the investigated CO_2 concentrations, AC60 shows the steeper curves and, hence, a faster CO_2 adsorption. This result is consistent with the results derived from the batch tests carried out in the manometric apparatus and can be ascribed to the wider pore dimension in the PSD of this sample (cf. Figure 2 and Table 1). In addition, the kinetic adsorption profiles of AC40 and AC60 sorbents practically overlap up to $Q^{out}_{CO_2}(t)/Q^{in}_{CO_2} \approx 0.1$, while a general smaller slope of the sigmoid is observed for AC20, likely due to a higher narrow micropore contribution. Moreover, for all the AC samples, an increase in CO_2 concentration fed to the column results in steeper breakthrough curves, possibly related to faster mass transfer phenomena taking place at higher driving force[32,42].

The differences in mass transfer rates can be better evaluated by introducing a time parameter $\Delta\tau = t_{0.7} - t_{0.1}$ (with $t_{0.1}$ and $t_{0.7}$ being the time for which $Q^{out}_{CO_2}(t)/Q^{in}_{CO_2}$=0.1 and 0.7, respectively) which is related to the slope of the linear part of the sigmoid: the smaller this parameter the steeper the breakthrough curve and consequently the faster the adsorption kinetics. The values of $\Delta\tau$ derived from the kinetic patterns for AC 20, 40 and 60 are listed in Table 3.

	AC20	AC40	AC60
Δτ (CO_2:1%), s	77	64	40
Δτ (CO_2:3%), s	60	49	33
Δτ (CO_2:5%), s	47	40	26
Δτ (CO_2:7%), s	41	36	23
Δτ (CO_2:9%), s	35	30	21
Δτ (CO_2:11%), s	31	28	19
Δτ (CO_2:13%), s	28	26	16
Δτ (CO_2:15%), s	25	24	15

Table 3. Comparison between Δτ values obtained from dynamic adsorption tests for AC20, AC40 and AC60 at different CO_2 concentration in the feed

Results confirm a significantly faster adsorption for AC60 for all CO_2 concentrations, while they allow highlighting that the differences between AC20 and AC40 tend to reduce when the CO_2 initial concentration increases and become negligible when it approaches the maximum investigated value (15%). For example, at 15% CO_2 in the feed, Δτ = 15, 24 and 25 s for AC 60, 40 and 20 respectively. Even if the kinetic differences between AC20 and AC40 are not so marked, particularly at higher pollutant concentration, the CO_2 capture process is generally slightly slower for AC20, if the time needed to reach equilibrium is considered. This result fully confirms the outcomes derived from the batch kinetic tests (Figure 3) and it testifies the perfect integration between these two analytical tests in the analysis of CO_2 adsorption on AC samples.

Further indications about the kinetic can be drawn out from the evaluation of the breakpoint times t_b, defined as the time for which $Q_{CO_2}^{out}(t)/Q_{CO_2}^{in}$=0.05. The highest values shown by AC20, coupled with a more gentle slope, proves that in the investigated experimental conditions, this sample has the highest CO_2 adsorption capacity, as discussed in the following.

The experimental data obtained on the dynamic apparatus were processed according to Eq. (1), in order to obtain useful thermodynamic indications about the behaviour of AC samples in the investigated conditions. Figure 5 depicts the adsorption isotherms obtained at 293 K in terms of molar equilibrium adsorption capacity as a function of CO_2 equilibrium partial pressure $P_{CO_2}^{eq}$.

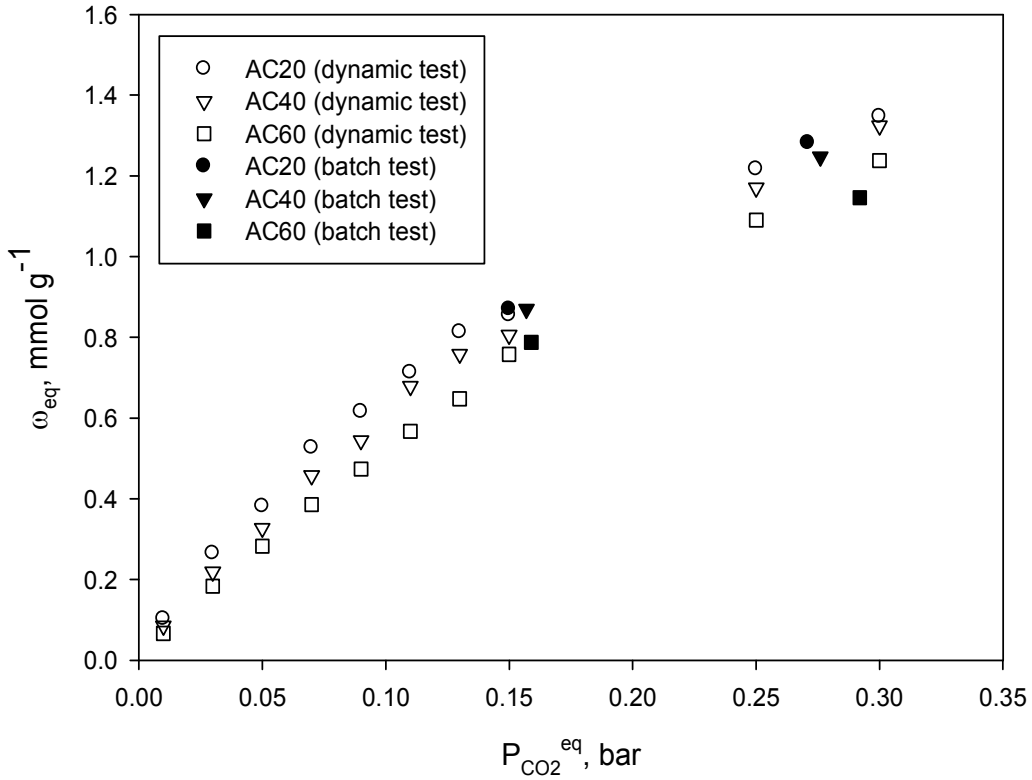

Figure 5. CO_2 adsorption isotherms on AC20, AC40 and AC60 as a function of CO_2 partial pressure (balance N_2). T=293 K and P=1 bar.

Experimental data clearly show that, in all the range of the investigated CO_2 partial pressure, the ranking of adsorption capacity is $\omega_{eq}(AC20)>\omega_{eq}(AC40)>\omega_{eq}(AC60)$. In particular, for a typical flue gas composition (i.e. CO_2 partial pressure ~ 0.15 bar) the adsorption capacity resulted to be 0.855, 0.806 and 0.758 mmol g^{-1}, respectively for AC20, AC40 and AC60. The experimental error of this series of data is always included in a ± 5% range, so that the observed ranking cannot be altered. It is worth to observe that the ranking is confirmed also in an extended range of CO_2 partial pressure (with respect to data reported in Figure 4). More interestingly, this extension allowed to compare the data obtained in the dynamic apparatus with the homologous data obtained in the batch apparatus, whose results were previously reported in Figures 3. To this aim, CO_2 equilibrium adsorption data as derived from batch tests were also included in Figure 5. A very good matching can be observed in terms of CO_2 adsorption capacity ranking, even if the different experimental conditions adopted for the two series of data did not allow a punctual comparison. Notwithstanding, it can be asserted with great confidence that the adsorption of N_2 on the synthesized AC samples can be considered as negligible. In fact, for each AC sample, pure CO_2 adsorption data (batch series) and CO_2+N_2 adsorption data (dynamic series) almost lies on the same adsorption isotherm. This result has very important implications in terms of practical utilization of these AC samples in a post combustion treatment of a real flue gas, since the competition of N_2 could seriously diminish CO_2 adsorption, affecting the efficiency of the process. However, it has to be underlined that typical flue-gas compositions include the presence of water, NOx, SOx and other contaminants which, despite of their low concentrations, can significantly influence CO_2 adsorption. Summarizing the considerations drawn from batch and dynamic adsorption tests at 293 K, it can be asserted that fixed bed experiments allow an accurate and simultaneous evaluation of both thermodynamic capture capacity and of the

dynamic response of the gas-solid system, with associated time-saving advantages for the proper selection of an activated carbon able to remove CO_2 from flue-gas under low operating pressure (<0.15 bar). Contextually, data from Figure 4 permit to consider AC20 as a better sorbent for practical application in large-scale adsorption unit aimed at mitigating CO_2-deriving global warming effect because, despite its slower adsorption kinetics, it showed a higher equilibrium adsorption capacity and a greater breakpoint time, hence it allows keeping CO_2 concentration at a lower level for higher operating time with respect to AC40 and AC60 sorbents.

Finally, an overall evaluation of the experimental results obtained in this work drives to the conclusion that the ranking observed in terms of CO_2 equilibrium adsorption capacity at 293 K (Figure 5) is not in line with the ranking observed for micropore and narrow micropore volumes (Table 1), for which AC60 results favoured. However, this evidence, apparently in contrast with the results reported in the literature on similar experimentations , must be evaluated together with the particular porous structure of the AC samples, which determines a combined dependence of CO_2 adsorption capacity both on CO_2 partial pressure and temperature. In fact, the determination of narrow micropore volume from CO_2 adsorption isotherm at 273 K (Figure 1) is made by considering the cumulative contribution corresponding to the entire CO_2 pressure range (0-1 bar). In these conditions, AC60 showed the highest CO_2 capture performances and, coherently, the highest narrow micropore volume. Conversely, until a CO_2 partial pressure <0.3 bar, AC20 showed the highest CO_2 adsorption capacity, also confirmed by experimental data realized at 293 K (Figure 3 and 5). Hence greater energetic interactions are determined by a higher adsorption potential, likely due to a narrower PSD shifted to narrow micropores. It is interesting to remark that these results were confirmed by comparing batch and dynamic data, realized in different experimental devices. Therefore, this work allowed determining the importance of a combined

application of different techniques (i.e. batch and dynamic tests) for a thorough comprehension of CO_2 adsorption on activated carbons and, in particular, for its practical application to the treatment of a flue gas in its typical conditions of temperature, pressure and CO_2 concentration.

4. Conclusions

The assessment of CO_2 adsorption capacity on a series of three different activated carbons, obtained from olives stones by physical and chemical activation at three different times i.e. 20, 40 and 60 hours, was experimentally carried out by a combination of batch and dynamic tests.

Preliminarily, a textural characterization of the samples (named AC20, AC40 and AC60) showed a monotonic increase of both the micropore and ultramicropore volume with the activation time, even if for CO_2 partial pressure lower than 0.3 bar the ranking for CO_2 adsorption capacity at 273 K is inverse, i.e. $\omega_{eq}(AC20)>\omega_{eq}(AC40)>\omega_{eq}(AC60)$. In order to deeper investigate the relationship between textural properties and CO_2 capture performances, kinetic and thermodynamic CO_2 adsorption tests were carried out at 293 K both in a batch apparatus (pure CO_2 tests) and in a dynamic apparatus, represented by a lab-scale fixed-bed column (CO_2+N_2 tests). In both the series of experiments, a very good agreement between homologous experimental results was observed, which allowed considering as negligible N_2 adsorption on all the AC samples. For CO_2 pressure <0.3 bar, the AC60 showed the lowest adsorption capacity but the fastest mass transfer phenomena, likely due to a remarkable greater contribution of mesopores and a wider micropore size distribution. Conversely, the AC20 sample exhibited the highest CO_2 adsorption capacity likely due to a greater contribution of smaller pores in the ultramicropore range. Interestingly, the ranking of CO_2 adsorption capacity in experimental conditions typical of a flue gas resulted to be $\omega_{eq}(AC20)>\omega_{eq}(AC40)>\omega_{eq}(AC60)$.

This ranking does not reflect the ranking observed in terms of ultramicropore volume (V_n(AC60)> V_n (AC40)> V_n (AC20)) determined by pure CO_2 isotherm at 273 K, but it is coherent with the adsorption capacity displayed by all the AC samples at 273 K in correspondence of a CO_2 pressure < 0.3 bar. Finally, this result highlights the importance of a deeper analysis of adsorption data for the determination of the factor affecting CO_2 adsorption performances. The different pore size distributions of the AC samples and in particular the higher contribution of ultramicropores observed for AC20 sample play a major role in determining a stronger interaction energy with CO_2 molecules at higher temperature and lower CO_2 partial pressure.

References

[1] Yang, H.; Xu, Z.; Fan, M.; Gupta, R.; Slimane, R.; Bland, A.; Wright, I. Progress in carbon dioxide separation and capture: A review. *J. Environ. Sci.* **2008**, *20*, 14-27.

[2] Figueroa, J.; Fout, T.; Plasynski, S.; McIlvried, H.; Srivastava, R. Advances in CO_2 capture technology-The U.S. Department of Energy's Carbon Sequestration Program. *Int. J. Greenh. Gas Con.* **2008**, *2*, 9-20.

[3] I. E. A. (IEA). Energy Technology Perspectives. **2010**. [Online]. Available: http://www.iea.org/techno/etp/etp10/English.pdf.

[4] Strube, R.; Manfrida, G. CO_2 capture in coal-fired power plants-Impact on plant performance. *Int. J. Greenh. Gas Con.* **2011**, *5*, 710-726.

[5] Brúder, P.; Svendsen, H. Capacity and kinetics of solvents for post-combustion CO_2 capture. *Energy Procedia* **2012**, *23*, 45-54.

[6] Herzog, H.; Meldon, J.; Hatton, A. Advanced post-combustion CO_2 capture. R*eport prepared for the Clean Air Task Force,* [Online]. Available: http://web.mit.edu/mitei/research/reports.html*,* 2009.

[7] Choi, S.; Drese, J.; Jones, C. Adsorbent materials for carbon dioxide capture from large anthropogenic point sources. *ChemSusChem* **2009**, *2*, 796-854.

[8] Samanta, A.; Zhao, A.; Shimizu, G.; Sarkar, P.; Gupta, R. Post-combustion CO_2 capture using solid sorbents: A review. *Ind. Eng. Chem. Res.* **2012**, *51*, 1438-1463.

[9] Abanades, J.; Rubin E.; Anthony, E. Sorbent cost and performance in CO_2 capture systems. *Ind. Eng. Chem. Res.* **2004**, *43*, 3462-3466.

[10] Erto, A.; Lancia, A.; Musmarra, D. A Real Adsorbed Solution Theory model for competitive multicomponent liquid adsorption onto granular activated carbon. *Micropor. Mesopor. Mater.* **2012**, *154*, 45-50.

[11] Whaby, A.; Ramos-Fernández, J.; Martínez-Escandell, M.; Sepúlveda-Escribano, A.; Silvestre Albero, J.; Rodríguez-Reinoso, F. High-surface-area carbon molecular sieves for selective CO_2 adsorption. *ChemSusChem* **2010**, *3*, 974-981.

[12] Sanz, R.; Calleja, G.; Arenciba, A.; Sanz-Pérez, E.S. Development of high efficiency adsorbents for CO_2 capture based on a double-functionalization method of grafting and impregnation. *J. Mater. Chem. A* **2013**, *1(6)*, 1956-1962.

[13] Wahby, A.; Silvestre-Albero, J.; Sepúlveda-Escribano, A.; Rodríguez-Reinoso, F. CO_2 adsorption on carbon molecular sieves. *Micropor. Mesopor. Mater.* **2012**, *164*, 280-287.

[14] Liu, Y.; Wilcox, J. Effects of Surface Heterogeneity on the Adsorption of CO_2 in microporous Carbons. *Environ. Sci. Technol.* **2012**, *46*, 1940-1947.

[15] Plaza, M.; Pevida, C.; Pis, J.; Rubiera, F. Evaluation of the cyclic capacity of low-cost adsorbent for post-combustion CO_2 capture. *Energy Procedia* **2011**, *4*, 1228-1234.

[16] Gomes, V.; Yee, K. Pressure swing adsorption for carbon dioxide sequestration from exhaust gases. *Sep. Purif. Technol.* **2002**, *28*, 161-171.

[17] Balsamo, M.; Budinova, T.; Erto, A.; Lancia, A.; Petrova, B.; Petrov, N.; Tsyntsarski, B. CO_2 adsorption onto synthetic activated carbon: kinetic, thermodynamic and regeneration studies. *Sep. Purif. Technol.* **2013**, *116*, 214-221.

[18] Sayari, A.;. Belmabkhout, Y; Serna-Guerrero, R. Flue gas treatment via CO_2 adsorption. *Chem. Eng. J.* **2011**, *171*, 760-774.

[19] Yang, R.; Liu, G.; Li, M.; Zhang, J.; Hao, X. Preparation and N_2, CO_2 and H_2 adsorption of super activated carbon derived from biomass source hemp (Cannabis sativa L.) stem.

Micropor. Mesopor. Mater. **2012**, *158*, 108–116.

[20] Shen, C.; Grande, C.; Li, P.; Yu, J.; Rodrigues, A. Adsorption equilibria and kinetics of CO_2 and N_2 on activated carbon beads. *Chem. Eng. J.* **2010,** *160*, 398-407.

[21] Marsh, H.; Rodríguez-Reinoso, F. *Activated Carbon*, Elsevier Science & Technology Books: Amsterdam, 2006.

[22] Ello, A. S.; de Souza, L. K.; Trokourey, A.; Jaroniec, M. Coconut shell-based microporous carbons for CO_2 capture. *Micropor. Mesopor. Mater.* **2013**, *180*, 280-283.

[23] Vargas, D. P.; Giraldo, L.; Moreno-Piraján, J. C. CO_2 adsorption on granular and monolith carbonaceous materials. *J. Anal. Appl. Pyrol.* **2012**, *96*, 146–152.

[24] Hao, W.; Björkman, E.; Lilliestråle, M.; Hedin, N. Activated carbons prepared from hydrothermally carbonized waste biomass used as adsorbents for CO_2. *Appl. Energ.* **2013,** *112*, 526-532.

[25] Vargas, D.; Giraldo, L.; Moreno-Piraján, J. Activated carbon for CO_2 adsorption obtained through the chemical activation of African palm stone. *Adsorpt. Sci. Technol.* **2013**, *31(9)*, 845-858.

[26] Lee, S. Y.; Park, S. J. Determination of the optimal pore size for improved CO_2 adsorption in activated carbon fibers. *J. Colloid Interface Sci.* **2013**, *389(1)*, 230–235.

[27] Vargas, D.; Giraldo, L.; Erto, A.; Moreno-Piraján, J. Chemical modification of activated carbon monoliths for CO_2 adsorption. *J. Therm. Anal. Calorim.* **2013**, *114(3)*, 1039-1047.

[28] Sevilla, M.; Parra, J.; Fuertes, A. Assessment of the role of micropore size and N-doping in CO_2 capture by porous carbons. *Appl. Mater. Interf.* **2013**, *5(13)*, 6360-6368.

[29] Sun, N.; Sun, C.; Liu, H.; Liu, J.; Stevens, L.; Drage, T.; Snape, C. E.; Li, K.; Wei W.; Sun, Y. Synthesis, characterization and evaluation of activated spherical carbon materials for CO_2 capture. *Fuel* **2013**, *113*, 854-862.

[30] Wickramaratne, N. P.; Jaroniec, M. Importance of small micropores in CO_2 capture by phenolic resin-based activated carbon spheres. J. *Mater. Chem. A* **2013**, *1*, 112-116.

[31] Yin, G.; Liu, Z.; Liu, Q.; Wu, W. The role of different properties of activated carbon in CO_2 adsorption. *Chem. Eng. J.* **2013**, *230*, 133-140.

[32] Balsamo, M.; Rodríguez-Reinoso, F.; Montagnaro, F.; Lancia, A., Erto, A. Highlighting the role of activated carbon particle size on CO_2 capture from model flue gas. *Ind. Eng. Chem.*

Res. **2013**, *52*, 12183−12191.

[33] Dantas, T. L. P.; Luna, F. M. T.; Silva Jr., I. J.; de Azevedo, D. C. S.; Grande, C. A.; Rodrigues, A. E.; Moreira, R. F. P. M. Carbon dioxide–nitrogen separation through adsorption on activated carbon in a fixed bed. *Chem. Eng. J.* **2011**, *169*, 11-19.

[34] García, S.; Gil, M.; Martín, C.; Pis, J.; Rubiera, F.; Pevida, C. Breakthrough adsorption study of a commercial activated carbon for pre-combustion CO_2 capture. *Chem. Eng. J.* **2011**, *171*, 549-556.

[35] Yong, Z.; Mata, V.; Rodrigues, A. Adsorption of carbon dioxide on chemically modified high surface area carbon-based adsorbents at high temperature. *Adsorption* **2001**, *7*, 41-50.

[36] Silvestre-Albero, A.; Silvestre-Albero, J.; Sepúlveda-Escribano, A.; Rodríguez-Reinoso, F. Ethanol removal using activated carbon: Effect of porous structure. *Micropor. Mesopor. Mater.* **2009**, *120*, 62–68.

[37] Garrido, J.; Linares-Solina, A.; Martin-Martinez, J.; Molina-Sabio, M.; Rodriguez-Reinoso, F.; Torregrosa, R. Use of nitrogen vs carbon dioxide in the characterization of activated carbons. *Langmuir* **1987**, *3*, 76-81.

[38] Martin-Martinez, J. M.; Torregosa-Macia, R.; Mittelmeijer-Hazeleger, M. C. Mechanisms of adsorption of CO_2 in the micropores of of activated anthracite. *Fuel* **1995**, *74*, 111-114.

[39] Casco, M.; Martínez-Escandell, M.; Silvestre-Albero, J.; Rodríguez-Reinoso, F. Effect of the porous structure in carbon materials for CO_2 capture at atmospheric and high-pressure. *Carbon* **2014**, *67*, 230-235.

[40] Cazorla-Amorós, D.; Alcañiz-Monge, J.; de la Casa-Lillo, M.; Linares-Solano, A. CO_2 as an adsorptive to characterize carbon molecular sieves and activated carbons. *Langmuir* **1998**, *14(16)*, 4589–4596.

[41] Zhang, Z.; Zhou, J.; Xing, W.; Xue, Q.; Yan, Z.; Zhuo, S.; Zhang Qiao, S. Critical role of small micropores in high CO_2 uptake. *Phys. Chem. Chem. Phys.* **2013**, *15*, 2523-2529.

[42] Ruthven, D. *Principles of adsorption and adsorption processes*; John Wiley & Sons:New York, 1984.

425

426